

Synthesis and stability of biomolecules in C-H-O-N fluids at extreme pressure-temperature conditions

Tao Li,¹ Nore Stolte,^{1,*} Renbiao Tao,² Dimitri A.
Sverjensky,³ Isabelle Daniel,⁴ and Ding Pan^{1,5,6,†}

¹*Department of Physics, Hong Kong University
of Science and Technology, Hong Kong, China*

²*Center for High Pressure Science and Technology
Advanced Research (HPSTAR), Beijing 100193, China*

³*Department of Earth and Planetary Sciences,
Johns Hopkins University, 3400 North Charles Street,
Baltimore, Maryland 21218, United States*

⁴*Universite Claude Bernard Lyon1,
LGL-TPE, UMR 5276, CNRS, Ens de Lyon,
Universite Jean Monnet Saint-Etienne, Villeurbanne, 69622, France*

⁵*Department of Chemistry, Hong Kong University
of Science and Technology, Hong Kong, China*

⁶*HKUST Shenzhen-Hong Kong Collaborative
Innovation Research Institute, Shenzhen, China*

(Dated: July 16, 2024)

Abstract

How life started on Earth is an unsolved mystery. There are various hypotheses for the location ranging from outer space to the seafloor, subseafloor or potentially deeper. Here, we applied extensive ab initio molecular dynamics (AIMD) simulations to study chemical reactions between NH_3 , H_2O , H_2 , and CO at pressures (P) and temperatures (T) approximating the conditions of Earth's upper mantle (*i.e.* 10 - 13 GPa, 1000 - 1400 K). Contrary to the previous assumptions that larger organic molecules might readily disintegrate in aqueous solutions at extreme P-T conditions, we found that many organic compounds formed without any catalysts and persisted in C-H-O-N fluids under these extreme conditions, including glycine, ribose, urea, and uracil-like molecules. Particularly, our free energy calculations showed that the C-N bond is thermodynamically stable at 10 GPa and 1400 K. Moreover, while the pyranose (six-membered-ring) form of ribose is more stable than the furanose (five-membered-ring) form at ambient conditions, we observed the predominant formation of the five-membered-ring form of ribose at extreme conditions, which is consistent with the exclusive incorporation of β -D-ribofuranose in RNA. We have uncovered a previously unexplored pathway through which the building blocks of biomolecules may have originated in early Earth and other planets. Our findings contribute to an evolving understanding of the fundamental conditions necessary for life to arise.

INTRODUCTION

The origin of life on Earth remains a profound scientific mystery. Numerous hypotheses have been put forward, but not a single one can explain all [1–3]. As early as ~ 150 years ago, Darwin proposed a “warm little pond” idea [4], which was later developed by Oparin and Haldane into the influential “primordial soup” theory in the 1920s [5], that is, the reactions of small molecules, such as CH_4 , NH_3 , H_2O , and CO_2 , to form the first organic compounds. This leads to the abiotic origin of life on early Earth. In 1953, the famous Miller-Urey experiment was conducted to test this hypothesis at the presence of electric discharge [6]. Inspired by the “primordial soup” theory, various prebiotic environments have been proposed for the origin of life, ranging from the outer space [7–9] to deep-sea hydrothermal vents [10, 11].

In those hypotheses, prebiotic chemistry typically happens at non-ambient conditions. The pressure (P) of hydrothermal vents, resulting from the interaction between seafloor and seawater producing hot fluids, is tens of megapascals depending on the depth of water, and the temperature (T) can reach 700 K. Those deep sea vents were considered to have suitable conditions for the origin of life [11], but previous studies also suggested that the high temperatures in the vents could readily degrade crucial biomolecules in aqueous solutions [12]. Shock recovery experiments successfully synthesized various biomolecules, where the pressure can reach tens of gigapascals and the temperature can rise to thousands of kelvins before releasing back to ambient conditions [13]; however, due to the dynamic nature of shock waves, samples do not reach thermodynamic equilibrium states, so the shock experiments are usually conducted to mimic the conditions of meteorite impacts on Earth [14]. It was commonly assumed that large biomolecules could not persist at both high hydrostatic pressures and high temperatures as found in Earth’s upper mantle, where pressures can reach up to ~ 13 GPa, accompanied by high temperatures of ~ 1700 K. In recent years, Otake et al. studied the stability of amino acids and their oligomerization at 1.0–5.5 GPa

and 453–673 K, and found that high-pressure conditions inhibited the decomposition of amino acids and small amino acids could be oligomerized up to pentamers; however, their experiments were conducted at the water-poor condition [15]. In aqueous solutions, there seems a strong thermodynamic drive towards the formation of amino acids dimers above 1.5 GPa and temperature above 423 K [16], in agreement with some experimental observations [17]. Previously, the fluids in Earth’s mantle were commonly modeled as simple mixtures of small unreactive volatile molecules, including H_2O , CO_2 , CO , CH_4 , and H_2 [18]. However, recent experimental and theoretical studies have revealed the significant roles played by chemical speciation, aqueous ions, and complexes in the supercritical geofluids within Earth’s lithosphere [19–25]. These findings have challenged the previous assumptions and shed light on the potential existence of larger organic molecules in Earth’s or other planets’ subsurface or even deeper.

It is very challenging to study the origin of life in laboratory settings due to the extreme environments and subsequent analyses. Atomistic simulations based on first principles have been applied to study prebiotic chemistry, offering significant molecular-level insights [26]. Saitta *et al.* applied ab initio molecule dynamics (AIMD) and metadynamics simulations to study the Miller-Urey experiment, and found unexpected reaction intermediates including formic acid and formamide [27]. Goldman *et al.* applied AIMD simulations to investigate the formation of prebiotic compounds from impact-induced shock compression of cometary ices followed by expansion to ambient conditions, and found that the impact of cometary ices could produce amino acids independently of atmospheric conditions and Earth minerals [28–30]. Note that the shock compression duration was less than 10 ps, so their simulations did not reach thermal equilibrium, and it is unknown whether the biomolecules can remain stable without being quenched to ambient conditions. AIMD simulations coupled with enhanced sampling techniques have also been applied to study the role of mineral surfaces in prebiotic chemistry [31–33]. Despite the numerous previous studies, the exploration of prebiotic chemistry at both high hydrostatic pressures and high temperatures largely remains

an uncharted territory.

Here, we applied extensive AIMD simulations to study the C-H-O-N fluids at 10–13 GPa and 1000–1400 K, the P-T conditions as found in the transition zone of Earth’s upper mantle. We discovered that a large range of organic molecules directly formed without any catalysts at extreme P-T conditions, including formamide, glycine, ribose, urea, and uracil-like molecules. Our free energy calculation suggested that the C-N bond is thermodynamically stable at 10 GPa and 1400 K. Our study provides valuable insights into a new potential avenue for the formation of building blocks of life and potentially for the origin of life within Earth’s and other planets’ interior, expanding our understanding of the conditions necessary for life to emerge.

RESULTS AND DISCUSSION

The simulation box initially contained 15 molecules of each of the following species: H_2O , H_2 , CO , and NH_3 (Figure S1). Those molecules are typical volatile compounds found in C-H-O-N fluids in reducing environments of Earth’s deep interior [18, 19], and are also abundant in interstellar space [34]. We conducted AIMD simulations at three P-T conditions, 10 GPa and 1000 K, 10 GPa and 1400 K, and 13 GPa and 1400 K, to evaluate how chemical products vary with P and T. Those P-T conditions are typically found at the bottom of Earth’s upper mantle. After more than 400 ps simulations at each P-T condition, we found about 100 different organic species. Here, we mainly focus on the formation of biotically relevant molecules, so we classify the organic molecules into six categories: “CN”, “ C_2N ”, “ CN_2 ”, “ C_2N_2 ”, “ C_3N_x ”, and “ C_4N_x ”, based on the numbers of carbon and nitrogen atoms, as shown in Table I. Fig. 1 shows the chemical structures of the representative species. Species with more than five carbon atoms were observed; however they are excluded at this stage due to their high instability and extremely short lifetime, typically lasting for only a few femtoseconds. The percents of these CN-containing species as a function of time at

three different P-T conditions are shown in Figure S3, which suggest that the concentrations of these species gradually stabilize over time.

At 10 GPa and 1000 K, most of the organic products belong to three main categories, as shown in Fig. 2(a). The “C₂N₂” species accounts for more than half of the CN-containing species, followed by the “CN” species, and finally “C₂N” species. Formamide is the primary product in the “CN” species [35]. It contains the peptide bond, which is a significant precursor for the production of more complex biomolecules, such as amino acids [36], nucleic acids, proteins, and even sugars [37, 38]. The “C₂N” species has the same CN-backbone (“-N-C-C-”) as glycine, suggesting that the “C₂N” species may be a potential reactant for the formation of amino acids. At this P-T condition, some of the “C₂N” species are not stable and can be transformed into the “C₂N₂” species by reacting with ammonia or ammonium ions, so the CN-backbone of “C₂N₂” species is “-N-C-C-N-”, and one interesting molecule is identified as alpha-hydroxy-glycineamide (α -HGA).

With increasing the temperature to 1400 K along the isobar at 10 GPa, all the six categories of organic products at this P-T condition were observed. Fractions of the “CN₂” and “C₄N_x” species are very small, while the other four species have similar fractions. Compared with 10 GPa and 1000 K, the portion of “C₂N₂” species becomes smaller, while there are more “C₂N” species. The “C₂N” species formed here also shares the same CN-backbone (“-N-C-C-”) with glycine. Notably, in the “C₂N” species, we found a molecule of α -hydroxyglycine, which can easily evolve into glycine [27]. The “C₂N₂” species has the CN-backbone of “-N-C-C-N-”, including α -HGA and oxamide. They are important organic molecules in the formation of the building blocks of peptides [39]. Among the “CN” species, formamide remains the most abundant one. Additionally, the “CN₂” species with the “-N-C-N-” backbone was observed, which did not typically form at 10 GPa and 1000 K. One representative product of this species is methanediane (CH₆N₂) [40], which was reported as a vital intermediate or precursor in the abiotic formation of nucleobases [41].

With increasing the pressure to 13 GPa at 1400 K, the “CN” species becomes dominating,

and the “C₂N₂” species comes next. For the “CN” species, besides formamide, some other crucial precursors for producing more complex biomolecules are identified, such as carbamic acid [42], isocyanic acid [43], and formimidic acid [44]. The “C₂N₂” species exhibits a distinct CN-backbone compared to the two solutions at 10 GPa, forming as “-C-N-C-N-”, which is present in allophanic acid. This acid plays a vital role in the synthesis of biomolecules, *e.g.*, uracil, and would be used as reactants in subsequent simulations of forming larger biomolecules. Surprisingly, the fraction of “C₂N” species sharply decreases, adopting a new CN-backbone structure of “-C-N-C-”, as observed in N-formylformamide [45]. This structural change makes it challenging for “C₂N” species formed here to evolve into glycine-like molecules or larger amino acids. In the “CN₂” species, we discovered the presence of urea molecule. Urea is closely related with biological processes [10] and considered to be an important condensation agent in prebiotic chemistry [46, 47], so it would also serve as a valuable reactant for investigating the reactions to larger biomolecules.

For all the three investigated P-T conditions, a common feature is that the “CN” and “C₂N₂” species are always the major components among the six CN-containing species. The lifetime distribution in Fig. 2 (b) shows that the “CN” and “C₂N₂” species could exist for a longer time at all three P-T conditions, suggesting that they are relatively more stable than other species.

Among these generated chemical products, formamide is a crucial precursor molecule that plays a vital role in the synthesis of biomolecules in prebiotic chemistry [35, 36, 48–51]. Thus, we first investigated the formation of formamide molecule. Fig. 3 (a) shows the different formation pathways at three P-T conditions, and detailed formation processes are displayed in Figure S4. At 10 GPa and 1000 K, the formation reaction begins with the dissociation of water molecules, generating OH⁻ and H⁺ ions in the aqueous solution. The encounter between an H⁺ ion and a CO molecule leads to the formation of a C-H bond and an aldehyde group (-CH=O). Subsequently, the aldehyde group reacts with a NH₃ molecule to generate a C-N bond, and then, one N-H bond breaks, ultimately producing formamide. At 10 GPa

and 1400 K, the formation process differs from that at 10 GPa and 1000 K. One N-H bond in NH_3 first breaks, leading to a dissociative amino group ($-\text{NH}_2$). The amino group then reacts with a CO molecule, forming the C-N bond. Later, a water molecule dissociates, providing a proton that ultimately contributes to the formation of the formamide molecule. At 13 GPa and 1400 K, the C-N bond is initially formed through the reaction between NH_3 and CO molecules. After a very short time, a dissociated proton from a water molecule is also bonded to the carbon atom, forming a C-H bond. Finally, by releasing a proton from the NH_3 group, the formamide molecule is generated. Despite the different formation pathways at three P-T conditions, we observed two common features: first, the reactants always have CO, H_2O , and NH_3 , and second, the reactions must involve the formation of C-N and C-H bonds and the breakage of N-H bonds.

For the generation of biomolecules in living matter, the formation of C-N bonds is the key step. We further applied the advanced sampling method (see details in the Methods section) to calculate the free energy profile of the C-N bond formation at three P-T conditions in Fig. 3(b). The collective variable (CV) is the distance between the carbon and nitrogen atoms. Our calculations show that the C-N bonds at 10 GPa, 1000 K and 13 GPa, 1400 K, whose lengths are 1.33 Å and 1.31 Å respectively, are at the metastable states. The free energy decreases upon dissociation of the C-N bond, indicating that breaking C-N bonds at these two P-T conditions are more thermodynamically favored. The free energy profiles suggest that the energy barriers of the C-N bond dissociation are 17.57 kcal/mol and 16.40 kcal/mol, at 10 GPa, 1000 K and 13 GPa, 1400 K, respectively. As a comparison, at 10 GPa and 1400 K, the free energy increases upon dissociation of the C-N bond (1.31 Å), and the energy barrier is 59.04 kcal/mol, indicating that the C-N bond is thermodynamically and kinetically stable at this P-T condition. The free energy result agrees with the data in Fig. 2, where there are more CN-containing species at 10 GPa and 1400 K than at the other two P-T conditions. Additionally, compared with the free energy profile at 10 GPa and 1000 K, there are two more energy minima at the C-N distance of 2.37 Å and 2.45 Å at 10 GPa,

1400 K and 13 GPa, 1400 K, respectively. The free energy increases upon the dissociation of the C-N pair, indicating that these two minima are thermodynamically stable. The C-N distances are larger than that of a typical C-N covalent bond, which implies the presence of an additional atom connecting the two. This is consistent with a wider variety of organic species at these two P-T conditions. Overall, our free energy calculations suggest that the C-N bond formation is favored at 10 GPa and 1400 K.

After studying the basic chemical products at three P-T conditions, we now turn to investigate the formation of large biomolecules as potential building blocks of life. Previous simulations have extensively studied glycine and the smallest amino acid under various conditions [27, 28, 52]. In our simulations at 10 GPa and 1400 K, we discovered α -hydroxyglycine, very similar to glycine. Fig. 4 (a) illustrates the process of forming α -hydroxyglycine from formamide. A proton attacked the formamide molecule, leading to the creation of a protonated formamide molecule, also known as an aminohydroxymethyl radical. Then, a CO_2 molecule reacts with the protonated formamide, resulting in the “-N-C-C-” backbone through forming a C-C bond. Finally, another proton is captured by a “-COO” group, ultimately yielding the α -hydroxyglycine molecule. In comparison to glycine, α -hydroxyglycine differs by having one hydrogen atom and an “-OH” group instead of two H atoms connecting to α -C. Glycine can be obtained if the “-OH” group is replaced by a hydrogen atom. During this process, the formation of the C-H bond is a crucial step. To explore appropriate P-T conditions for the possible synthesis of glycine, we calculated the free energy as a function of the C-H distance in Fig. 4 (b). Considering that the CN-backbone of the “ C_2N ” species at 13 GPa - 1400 K is “-C-N-C-”, different from the CN-backbone in the glycine molecule, we did not consider this P-T condition. We can see that the free energy minima is at 1.07 Å for both 10 GPa, 1000 K and 10 GPa, 1400 K, and the energy barriers to break the C-H bond are 21.91 kcal/mol and 22.04 kcal/mol, respectively, which are very similar. After the C-H bond dissociation, the free energy increases more at 10 GPa and 1400 K (6.76 kcal/mol) than at 10 GPa and 1000 K (2.63 kcal/mol), indicating that the C-H bond is more favored at the

former P-T condition.

To study the reaction from α -hydroxyglycine to glycine at extreme P-T conditions, we set up a new simulation box containing 5 α -hydroxyglycine, 10 H_2 , and 10 H_2O molecules, as shown in Fig. 4(c) and performed AIMD simulations at 10 GPa and 1400 K. Initially, two α -hydroxyglycine molecules combine to form one molecule, but later dissociate to dehydroglycine and glyoxylic acid after ~ 28 ps. As the simulation goes on, the C=N double bond in the dehydroglycine molecule receives two protons and finally dehydroglycine becomes glycine at ~ 38 ps.

Both proteins and DNA are widely recognized as the important biomolecules for building blocks of life. However, the question of which one came first in the emergence of life remains a topic of debate. This is due to the fact that the replication of DNA relies on the catalytic activity of enzymes, which are a type of proteins. Conversely, the production of proteins also needs the guidance of DNA, resulting in a chicken-and-egg dilemma. To solve this problem, a hypothesis known as “the RNA world” was proposed, which believed that RNA may occur earlier than DNA and protein [53, 54]. During this stage, the RNA not only have the ability to reproduce themselves and carry genetic information, but also could catalyze certain biological reactions in life activities like enzymes [55, 56]. Thus, the synthesis of RNA plays an critical role in the early stage of the origin of life. RNA is composed of ribose sugar, four kinds of nucleobases, and a phosphate group. Considering that our simulations only involve the carbon, hydrogen, oxygen, and nitrogen elements, we then explored whether the ribose and nucleobases could be synthesized under extreme conditions.

We first considered ribose ($\text{C}_5\text{H}_{10}\text{O}_5$). The formose reaction is a well-known prebiotic pathway for synthesizing ribose from formaldehyde (CH_2O) [57]. Our simulations have generated a few relevant hydrocarbon products (shown in Figures S5 and S6), including formaldehyde molecule (number 1 in Figure S5), which was later chosen as the primary reactant. Additionally, to facilitate the synthesis process, the reactants also included a “ C_2 ” molecule, (Z)-ethene-1,2-diol ($\text{C}_2\text{H}_4\text{O}_2$, number 7 in Figure S5). Initially, we constructed a

simulation box consisting of 10 (Z)-ethene-1,2-diol molecules and 5 formaldehyde molecules (Figure S7). After ~ 76 ps, a “C₅” molecule was formed at ~ 10 GPa and 1400 K. However, it did not transform into the structure of ribose after an extended time. We further tried to add other reactants to the simulation box, and found that after adding 5 water molecules, the ribose molecule appeared, indicating the importance role of water in the formation of ribose. The reaction process is shown in Fig. 5 (a), where the formaldehyde and “C₂” molecules react to form a “C₃” molecule, which then combines with another “C₂” molecule to form a “C₅” molecule. This “C₅” molecule then evolves into the open-chain form of ribose at ~ 19 ps.

We calculated the free energy landscape in Fig. 5 (b), where two C-C distances were selected as collective variables labelled as CV1 and CV2. For CV1, two carbon atoms come from formaldehyde and a “C₂” molecule, respectively, which are labeled as C1. While for CV2, two carbon atoms are from two different “C₂” molecules, marked as C2. The free energy landscape shows a clear energy minimum corresponding to the formation of ribose, but the C-C distance at this minimum is larger than a typical C-C bond distance. We examined the biased molecular dynamics trajectories and found that the carbon backbone of the generated ribose molecule has the C1-C2-C1-C2 structure. By measuring the distances of C1-C1 and C2-C2, we confirmed that they are consistent to the distances observed in the free energy landscape. We also randomly selected another initial configuration to confirm that the ribose molecule is thermodynamically stable, as shown in Figure S8.

Previous studies showed that the cyclic forms of ribose are abundant in aqueous solutions at room temperature [58]. However, the cyclic forms of ribose were not detected in our simulations (Fig. 5 (a)). The limited size of our simulation boxes may restrict the configuration changes of ribose, thereby decreasing the likelihood of the C4’ or C5’ hydroxyl group attacking the C1’ aldehyde group. This limitation is unfavorable for the production of the furanose form (five-membered ring) or pyranose form (six-membered ring). To further study the cyclic formation mechanism, we carried a few additional simulations and finally

chose the curved open-chain ribose molecules obtained from our previous simulations, as it appears that the C4' or C5' hydroxyl group has a greater chance of reacting with the C1' aldehyde group under pressure. We built a new simulation box containing three of these ribose molecules together with 18 water molecules. After about 36 ps, we found the direct formation of a furanose form of ribose. Fig. 5 (c) shows the mechanism of ring formation. In this process, the C4' hydroxyl group first loses a hydrogen atom, leaving a carbonyl group. The oxygen atom then attacks C1' to form the ring, and finally, the carbonyl group on C1' receives a dissolved proton in the solution to generate the five-membered ribose ring. Interestingly, no six-membered ring was found in our simulations at 10 GPa and 1400 K.

We further applied free energy calculations to study the formation ability of five- and six-membered ribose rings at ~ 10 GPa and 1400 K. We chose two C-O distances as the CVs for the two rings, as shown in Fig. 5 (d). The energy minima are at the C-O distance of 1.37 Å for the two ribose forms, indicating the formation of C-O bonds and the rings. Besides, the formation of the C-O bonds lowers the free energy by 11.57 kcal/mol for the five-membered ribose ring and 5.85 kcal/mol for the six-membered ribose ring, indicating that the ring formation is thermodynamically more stable and the furanose form of ribose is more favored than the pyranose form at ~ 10 GPa and 1400 K. The free energy result explained why the the pyranose form of ribose is absent in our AIMD simulations. The spacial limitation under high pressure may hinder the formation of larger cyclic forms of molecules, so the energy barrier of forming a five-membered ring is lower than that of a six-membered ring.

Note that at ambient conditions, the naturally-occurring ribose exists as a mixture of cyclic forms in equilibrium with its open-chain form in aqueous solutions, and the pyranose form of ribose is the predominant conformation, accounting for approximately 70% [59, 60]. However, despite the thermodynamic stability of the pyranose form of ribose over the furanose form at ambient conditions, the exclusive constituent of the carbohydrate backbone of RNA remains the furanose form of ribose. The reason behind it is still unknown. There

are several hypotheses proposed to explain this preference, including silicate(borate)/ribose complexes [61, 62] and temperature gradients [60]. Our finding suggests that extreme P-T conditions may also generate the necessary component for assembling RNA molecules. Consequently, it highlights the potential role of upper mantle environment in facilitating the emergence and development of RNA-based life.

We then shifted our attention to the chemical evolution of nucleobases, which are another essential building blocks of genetic information. There are five naturally-occurring nucleobases: adenine (A), cytosine (C), guanine (G), thymine (T), and uracil (U). Of these, uracil is unique to RNA, so our studies primarily focused on investigating the formation of uracil molecules under extreme conditions. We first studied the formation of the open-chain “C₄N₂” molecule which has the same CN-backbone as the open-chain form of uracil, as shown in Fig. 6 (a). Previous experimental studies on the origins of life have suggested that formamide is a crucial molecule for the prebiotic formation of nucleobases, in the presence of mineral or metal oxide catalysts [35], heating[48], and high-energy free radicals [51, 63], so here we also first chose formamide as a reactant. However, after about 144 ps, we did not observe the formation of the “C₄N₂” molecule at 10 GPa and 1400 K, suggesting that it may be difficult for small molecules to directly synthesize uracil in the AIMD simulations (Figure S9). Later, we chose the chemical reactants that have closer structural similarities to the “C₄N₂” molecule. The reactant molecules, including “C₄N”, “C₃N₂”, “C₂N₂”, and “C₃”, were generated from our first-stage AIMD simulations. A recent study suggested that uracil could be synthesized from the reactions between urea and “C₃” molecules [64], so we specifically selected the C₃H₄O₄ molecule (number 10 in Figure S5) and the urea molecule (CH₄N₂O, number 11 in Fig. 1) as reactants. The simulation results are presented in Figure S10. However, regardless of the inclusion of water molecules or the application of different pressure conditions, we did not observe any “C₄N₂” molecules with the CN-backbone of the open-chain form of uracil. Then we tried to find another pathways and conducted six more AIMD simulations to investigate the possibility of forming uracil through reactions involving

above-mentioned molecules at various pressures and 1400 K (see Figures S11, S12 and S14).

We found that, the $C_4H_8N_2O_2$ molecule, N-(((λ^3 -methyl)amino)methyl)-2-hydroxy-2 λ^3 -ethanamide (labeled as “ C_4N_2 -1”), which has the same CN-backbone as the open-chain form of uracil, was formed in the simulation box consisting of 3 $C_3H_8N_2O_2$ (number 15 in Fig. 1), 10 H_2O , 10 H_2 , and 10 CO molecules, at ~ 10 GPa and 1400 K. The formation process is provided in Figure S13. Like ribose, the “ C_4N_2 -1” molecule retained its open-chain form after an extended simulation of ~ 108 ps.

To study the ring formation of uracil, we also selected the “ C_4N_2 -1” molecule with large curvature and built a simulation box containing 6 “ C_4N_2 -1” and 6 water molecules. Fig. 6 (b) shows that all the “ C_4N_2 -1” molecules reacted. At 5.6 GPa and 1400 K, open-chain “ C_4N_2 -1” molecules became five-membered and six-membered rings within a shorter time of about 3.6 ps. Particularly, the elements in the six-membered-ring molecule are the same as those in uracil as shown in Fig. 6(a). At 9.3 GPa and 1400 K, the same six-membered-ring molecule was also formed. These simulations suggest that it is possible for the open-chain form of uracil to transform into the cyclic form. We further performed free energy calculations to analyze this ring formation reaction. We first chose the distance between the head and tail carbon atoms in the open-chain form of uracil as the CV. The enhanced sampling simulation at ~ 10 GPa and 1400 K produced the same six-membered-ring molecule as in our unbiased simulations. Note that the free energy profile suggests that the cyclic form is in a metastable state, as shown in Fig. 6(b).

Later we chose allophanic acid ($C_2H_4N_2O_3$, number 13 in Fig. 1) and (Z)-ethene-1,2-diol ($C_2H_4O_2$, number 7 in Figure S5) as reactants, and built a new simulation box containing 5 $C_2H_4N_2O_3$, 5 $C_2H_4O_2$, and 10 H_2 , as shown in Fig.6 (c). At ~ 10 GPa and 1400 K, a “ C_5N_2 ” molecule, 3-(3-carboxyureido)-2,3-dihydroxypropanoic acid, was formed at around 28.8 ps, This molecule has the same CN-backbone as the open-chain form of thymine (T). As the simulation continued, a “ C_4N_2 ” molecule, 2,3-dihydroxy-3-ureidopropanoic acid, labeled as “ C_4N_2 -2”, was formed, which has the same CN-backbone as the open-chain form of uracil.

The formation process of these two kinds of molecules are shown in Figure S15. We further performed an enhanced sampling simulation to analyze the ring formation process at ~ 10 GPa and 1400 K. The simulation box has one “C₄N₂-2” molecule and 32 water molecules, as shown in Fig. 6 (c). Finally, a uracil-like molecule, called uracil glycol, was synthesized, which has a uracil ring. The free energy curve in Fig. 6 (c) shows that the cyclic form is more stable than the open-chain form, indicating that the uracil-like molecule is possible to form in geological C-H-O-N fluids at extreme P-T conditions. The uracil-like molecule can then serve as a precursor for the synthesis of other three types of nucleobases, providing the necessary components for forming RNA molecules.

Geochemical evidence of biotic activity suggests that the emergence of life can be traced back to as early as 3.8 billion years ago [65]. The modern style of plate tectonics may have started about 3.2 billion years ago [66], but some form of plate tectonics may have already been active around 4.0 billion years ago. and these tectonic activities might carry water, carbon, and other volatile substances down into the mantle [67–71]. Because of reducing environments in early Earth’s mantle [72], oxidized carbon and nitrogen can be reduced to CO and NH₃/NH₄⁺, respectively [73](see Figure S16), and they may further synthesize to become key building blocks of life, which may reach the surface of early Earth. Our findings also have important implications for organic molecules in interstellar space. The reactant molecules H₂O, H₂, CO and NH₃ largely exist in interstellar clouds and circumstellar shells, together with more than 200 complex organic species, such as aldehydes, alcohols, acids, amines and carboxamides [34]. It is unclear how those complex organic species are generated. Our current study suggests that the extreme pressure and temperature inside giant planets and their moons [74, 75], like Jupiter and Saturn, may help to synthesize those complex organic molecules [76–78].

CONCLUSIONS

Extensive AIMD simulations have been performed to investigate the chemical reactions of small proto-organic molecules under the extreme P-T conditions. Three corresponding P-T systems were considered, *i.e.*, 10 GPa - 1000 K, 10 GPa - 1400 K, and 13 GPa - 1400 K. The simulation results have revealed the potential formation of substantial quantities of organic matter without any catalysts, with the composition and abundance of CN-containing species being profoundly influenced by the specific P-T conditions. Notably, formamide, recognized as a crucial precursor in the production of biomolecules, is observed to readily form under extreme P-T conditions, and its formation pathways are compared across different P-T conditions. Furthermore, free energy calculations have confirmed that the 10 GPa - 1400 K condition is particularly favorable for the generation and preservation of CN-containing compounds.

Using the molecules formed, we have further explored the formation process of large biomolecules that are directly related to the building blocks of life. Remarkably, glycine, ribose, urea, and uracil-like molecules are successfully synthesized under extreme conditions in our AIMD simulations, thereby providing initial insights into the formation of organic compounds critical to the emergence of life. More importantly, different from that the six-membered ring of ribose is the majority in solutions at ambient conditions, it is found that formation of five-membered ring form of ribose is more favored at extreme P-T conditions, which could provide the necessary components for the generation of RNA molecules. Moreover, these compounds have the potential to be transported to Earth’s surface through geological activities, such as mantle convection, consequently contributing to the origins of life. The complex organic species found in interstellar space may be also related to the chemical processes inside giant planets and their moons at extreme P-T conditions. Our comprehensive studies present a novel perspective extending the cradle of life planetary interiors. The findings underscore the profound impact of extreme P-T conditions on the

formation of organic matter and provide valuable insights into the mechanisms underlying the emergence of life within planetary bodies.

METHODS

Ab initio molecular dynamics simulations (AIMD)

We carried out AIMD simulations with the Born-Oppenheimer approximation using the Qbox code [79]. We applied the PBE exchange-correlation functional in density functional theory [80]. It is known that the PBE functional may be insufficient to describe aqueous solutions at ambient conditions, but our previous studies found that it works better at extreme P-T conditions than at ambient conditions [20, 22, 24, 25], and many other studies also showed that this semi-local functional is reliable to study matter under extreme conditions [81–83]. We used the ONCV pseudopotentials [84], and the Bussi-Donadio-Parrinello (BDP) thermostat, with a relaxation time of 24.2 fs, to control the temperature [85]. To facilitate a larger time step of 0.24 fs, deuterium atoms were used in place of hydrogen atoms in our simulations. The simulation boxes have periodic boundary conditions. We first performed NPT simulations to achieve the desired pressures, configuring the plane-wave energy cutoff to 85 Ry and the energy cutoff for stress confinement potential to 70 Ry. We applied the simulation box sizes (Table S1) obtained from NPT simulations in the following NVT simulations for production runs, where the plane-wave energy cutoff was 65 Ry. During NVT simulations, we selected random time points to carry out independent simulations with energy cutoff of 85 Ry to monitor pressure (Figure S2). Our total AIMD simulation time exceeds 2.5 ns.

Free-energy calculations by coupling AIMD simulations with enhanced sampling

To compute the free-energy landscape, we employed the adaptive biasing force method (ABF) [86] as implemented in the software package SSAGES [87] coupled with Qbox code. Unlike other advanced sampling methods that introduce biases into the energy, this method aims to flatten the generalized force. The running average of the force in the k th bin along the reaction coordinate ξ is calculated as:

$$F_{\xi}(N_{\text{step}}, k) = \frac{1}{\nu(N_{\text{step}}, k)} \sum_{i=1}^{\nu(N_{\text{step}}, k)} F_i(t_i^k) \quad (1)$$

$$F_i(t_i^k) = \frac{d}{dt} \left(M_{\xi} \frac{d\xi}{dt} \right) \bigg|_{t_i^k} \quad (2)$$

where $\nu(N_{\text{step}}, k)$ is the number of samples collected in the k th bin after N_{step} steps, $F_i(t_i^k)$ is the i th force sample at the time t_i^k , M is the mass matrix. The bias force $-(\nabla \xi) F_{\xi}(N_{\text{step}}, k)$ is added to the calculation until the free energy landscape is flat. We finally integrated the total biased force to get the free energy. For example, the free energy $\Delta A_{a \rightarrow b}$ between two states a and b is calculated as:

$$\Delta A_{a \rightarrow b} = - \int_{\xi_a}^{\xi_b} F_{\xi} d\xi \approx - \frac{\xi_b - \xi_a}{k_{\text{max}}} \sum_{k=1}^{k_{\text{max}}} F_{\xi}(N_{\text{step}}, k)$$

SUPPORTING INFORMATION

Details of the simulations, the percentage of C-N containing species over time, the hydrocarbon products, the free energy calculations, other strategies for the formation of ribose and uracil, and their ring structures, compositions of fluids at different oxygen fugacity.

ACKNOWLEDGEMENTS

This work was supported by the Croucher Foundation through the Croucher Innovation Award, Hong Kong Research Grants Council (Projects GRF-16301723, GRF-16306621, and

C6021-19EF), National Natural Science Foundation of China through the Excellent Young Scientists Fund (22022310), and the Hetao Shenzhen/Hong Kong Innovation and Technology Cooperation (HZQB-KCZYB-2020083). R.T. would like to acknowledge support from the Original Exploration Plan-Key project (42150104). Contributions by D.A.S. constitute material based upon work supported by the U.S. Department of Energy, Office of Science, Basic Energy Sciences, Geosciences program under Award Number DE-SC0019830 as well as NSF Petrology and Geochemistry Grant Number 2032039. Part of this work was carried out using computational resources from the National Supercomputer Center in Guangzhou, China.

* Present address: Lehrstuhl für Theoretische Chemie, Ruhr-Universität Bochum, 44780 Bochum, Germany

† dingpan@ust.hk

- [1] Orgel, L. E. The origin of life on the earth. *Sci. Am.* **271**, 76–83 (1994).
- [2] Mann, S. The origins of life: old problems, new chemistries. *Angew. Chem., Int. Ed.* **52**, 155–162 (2013).
- [3] Sutherland, J. D. Opinion: Studies on the origin of life—the end of the beginning. *Nat. Rev. Chem.* **1**, 0012 (2017).
- [4] Darwin, C. To jd hooker 1 february [1871]. *Darwin Correspondence Project, Cambridge University Library, Cambridge*. <https://www.darwinproject.ac.uk/letter/DCP-LETT-7471.xml> (1871).
- [5] Oparin, A. I. *The origin of life on the earth*. (Academic Press, 1957).
- [6] Miller, S. L. A production of amino acids under possible primitive earth conditions. *Science* **117**, 528–529 (1953).

- [7] Ziurys, L. M. The chemistry in circumstellar envelopes of evolved stars: Following the origin of the elements to the origin of life. *Proc. Natl. Acad. Sci.* **103**, 12274–12279 (2006).
- [8] Sandford, S. A., Nuevo, M., Bera, P. P. & Lee, T. J. Prebiotic astrochemistry and the formation of molecules of astrobiological interest in interstellar clouds and protostellar disks. *Chem. Rev.* **120**, 4616–4659 (2020).
- [9] Krasnokutski, S., Chuang, K.-J., Jäger, C., Ueberschaar, N. & Henning, T. A pathway to peptides in space through the condensation of atomic carbon. *Nat. Astron.* **6**, 381–386 (2022).
- [10] Daniel, I., Oger, P. & Winter, R. Origins of life and biochemistry under high-pressure conditions. *Chem. Soc. Rev.* **35**, 858–875 (2006).
- [11] Martin, W., Baross, J., Kelley, D. & Russell, M. J. Hydrothermal vents and the origin of life. *Nat. Rev. Microbiol.* **6**, 805–814 (2008).
- [12] Miller, S. L. & Bada, J. L. Submarine hot springs and the origin of life. *Nature* **334**, 609–611 (1988).
- [13] Sekine, T. *Shock Synthesis and Evolution of Biomolecules: Organic Materials Synthesis and Origin-of-Life-Related Biomolecules*, 81–88 (Springer Nature Singapore, Singapore, 2024). URL https://doi.org/10.1007/978-981-97-3729-1_6.
- [14] Furukawa, Y., Sekine, T., Oba, M., Kakegawa, T. & Nakazawa, H. Biomolecule formation by oceanic impacts on early earth. *Nat. Geosci.* **2**, 62–66 (2009).
- [15] Otake, T. *et al.* Stability of amino acids and their oligomerization under high-pressure conditions: implications for prebiotic chemistry. *Astrobiology* **11**, 799–813 (2011).
- [16] Robinson, K. J. *et al.* Quantifying the extent of amide and peptide bond synthesis across conditions relevant to geologic and planetary environments. *Geochim. Cosmochim. Acta* **300**, 318–332 (2021).
- [17] Pedreira-Segade, U., Hao, J., Montagnac, G., Cardon, H. & Daniel, I. Spontaneous polymerization of glycine under hydrothermal conditions. *ACS Earth Space Chem.* **3**, 1669–1677 (2019).

- [18] Zhang, C. & Duan, Z. A model for C–O–H fluid in the Earth’s mantle. *Geochim. Cosmochim. Acta* **73**, 2089–2102 (2009).
- [19] Manning, C. E., Shock, E. L. & Sverjensky, D. A. The chemistry of carbon in aqueous fluids at crustal and upper-mantle conditions: experimental and theoretical constraints. *Rev. Mineral. Geochem.* **75**, 109–148 (2013).
- [20] Pan, D., Spanu, L., Harrison, B., Sverjensky, D. A. & Galli, G. Dielectric properties of water under extreme conditions and transport of carbonates in the deep Earth. *Proc. Natl. Acad. Sci.* **110**, 6646–6650 (2013).
- [21] Sverjensky, D., Daniel, I. & Brovarone, A. V. The changing character of Carbon in fluids with pressure: Organic geochemistry of Earth’s upper mantle fluids. *Carbon in Earth’s Interior* 259–269 (2020).
- [22] Pan, D. & Galli, G. The fate of carbon dioxide in water-rich fluids under extreme conditions. *Sci. Adv.* **2**, e1601278 (2016).
- [23] Abramson, E. H., Bollengier, O. & Brown, J. M. The water-carbon dioxide miscibility surface to 450 C and 7 GPa. *Am. J. Sci.* **317**, 967–989 (2017).
- [24] Stolte, N. & Pan, D. Large presence of carbonic acid in CO₂-rich aqueous fluids under Earth’s mantle conditions. *J. Phys. Chem. Lett.* **10**, 5135–5141 (2019).
- [25] Stolte, N., Yu, J., Chen, Z., Sverjensky, D. A. & Pan, D. Water–gas shift reaction produces formate at extreme pressures and temperatures in deep earth fluids. *J. Phys. Chem. Lett.* **12**, 4292–4298 (2021).
- [26] Pérez-Villa, A., Pietrucci, F. & Saitta, A. M. Prebiotic chemistry and origins of life research with atomistic computer simulations. *Phys. Life Rev.* **34**, 105–135 (2020).
- [27] Saitta, A. M. & Saija, F. Miller experiments in atomistic computer simulations. *Proc. Natl. Acad. Sci.* **111**, 13768–13773 (2014).
- [28] Goldman, N., Reed, E. J., Fried, L. E., William Kuo, I.-F. & Maiti, A. Synthesis of glycine-containing complexes in impacts of comets on early earth. *Nat. Chem.* **2**, 949–954 (2010).

- [29] Goldman, N. & Tamblyn, I. Prebiotic chemistry within a simple impacting icy mixture. *J. Phys. Chem. A* **117**, 5124–5131 (2013).
- [30] Koziol, L. & Goldman, N. Prebiotic hydrocarbon synthesis in impacting reduced astrophysical icy mixtures. *Astrophys. J.* **803**, 91 (2015).
- [31] Nair, N. N., Schreiner, E. & Marx, D. Glycine at the pyrite- water interface: the role of surface defects. *J. Am. Chem. Soc.* **128**, 13815–13826 (2006).
- [32] Pollet, R., Boehme, C. & Marx, D. Ab initio simulations of desorption and reactivity of glycine at a water-pyrite interface at “iron-sulfur world” prebiotic conditions. *Origins Life Evol. Biospheres* **36**, 363–379 (2006).
- [33] Schreiner, E., Nair, N. N., Wittekindt, C. & Marx, D. Peptide synthesis in aqueous environments: the role of extreme conditions and pyrite mineral surfaces on formation and hydrolysis of peptides. *J. Am. Chem. Soc.* **133**, 8216–8226 (2011).
- [34] Guélin, M. & Cernicharo, J. Organic molecules in interstellar space: Latest advances. *Front. Astron. Space Sci.* **9**, 787567 (2022).
- [35] Saladino, R., Crestini, C., Pino, S., Costanzo, G. & Di Mauro, E. Formamide and the origin of life. *Phys. Life Rev.* **9**, 84–104 (2012).
- [36] Pietrucci, F. & Saitta, A. M. Formamide reaction network in gas phase and solution via a unified theoretical approach: Toward a reconciliation of different prebiotic scenarios. *Proc. Natl. Acad. Sci.* **112**, 15030–15035 (2015).
- [37] Saladino, R., Botta, G., Pino, S., Costanzo, G. & Di Mauro, E. Genetics first or metabolism first? the formamide clue. *Chem. Soc. Rev.* **41**, 5526–5565 (2012).
- [38] Halfen, D., Ilyushin, V. & Ziurys, L. Formation of peptide bonds in space: a comprehensive study of formamide and acetamide in Sgr B2 (N). *Astrophys. J.* **743**, 60 (2011).
- [39] Ligterink, N. *et al.* The formation of the building blocks of peptides on interstellar dust grains. *Proc. Int. Astron. Union* **15**, 216–219 (2019).

- [40] Carballeira, L. & Pérez-Juste, I. Role of the anomeric effect in methanediamines in the gas phase and aqueous solutions. *J. Comput. Chem.* **22**, 135–150 (2001).
- [41] Marks, J. H., Wang, J., Fortenberry, R. C. & Kaiser, R. I. Preparation of methanediamine ($\text{CH}_2(\text{NH}_2)_2$)—A precursor to nucleobases in the interstellar medium. *Proc. Natl. Acad. Sci.* **119**, e2217329119 (2022).
- [42] Tossell, J. What happens at the microscopic level when CO_2 reacts with ammonia or amines in solution or on cryogenic surfaces? *Energy Environ. Sci.* **3**, 1079–1091 (2010).
- [43] Belson, D. & Strachan, A. Preparation and properties of isocyanic acid. *Chem. Soc. Rev.* **11**, 41–56 (1982).
- [44] Pranata, J. & Davis, G. D. Computational investigations of reactive intermediates in the acid-catalyzed proton exchange in formamide. *J. Phys. Chem.* **99**, 14340–14346 (1995).
- [45] Sanz, P., Mó, O., Yáñez, M. & Elguero, J. The effects of C by N replacement on the hydrogen bonding of malonaldehyde: N-formylformimidic acid, N-(hydroxymethyl) formamide and related compounds. *Phys. Chem. Chem. Phys.* **11**, 762–769 (2009).
- [46] Burcar, B. *et al.* A stark contrast to modern earth: Phosphate mineral transformation and nucleoside phosphorylation in an iron-and cyanide-rich early Earth scenario. *Angew. Chem. Int. Ed.* **131**, 17137–17143 (2019).
- [47] Gull, M., Omran, A., Feng, T. & Pasek, M. A. Silicate-, magnesium ion-, and urea-induced prebiotic phosphorylation of uridine via pyrophosphate; revisiting the hot drying water pool scenario. *Life* **10**, 122 (2020).
- [48] Enchev, V. *et al.* Chemical evolution: from formamide to nucleobases and amino acids without the presence of catalyst. *J. Biomol. Struct. Dyn.* **39**, 5563–5578 (2021).
- [49] Saladino, R. *et al.* Meteorite-catalyzed syntheses of nucleosides and of other prebiotic compounds from formamide under proton irradiation. *Proc. Natl. Acad. Sci.* **112**, E2746–E2755 (2015).
- [50] Rios, A. C. Impact synthesis of the RNA bases. *Proc. Natl. Acad. Sci.* **112**, 643–644 (2015).

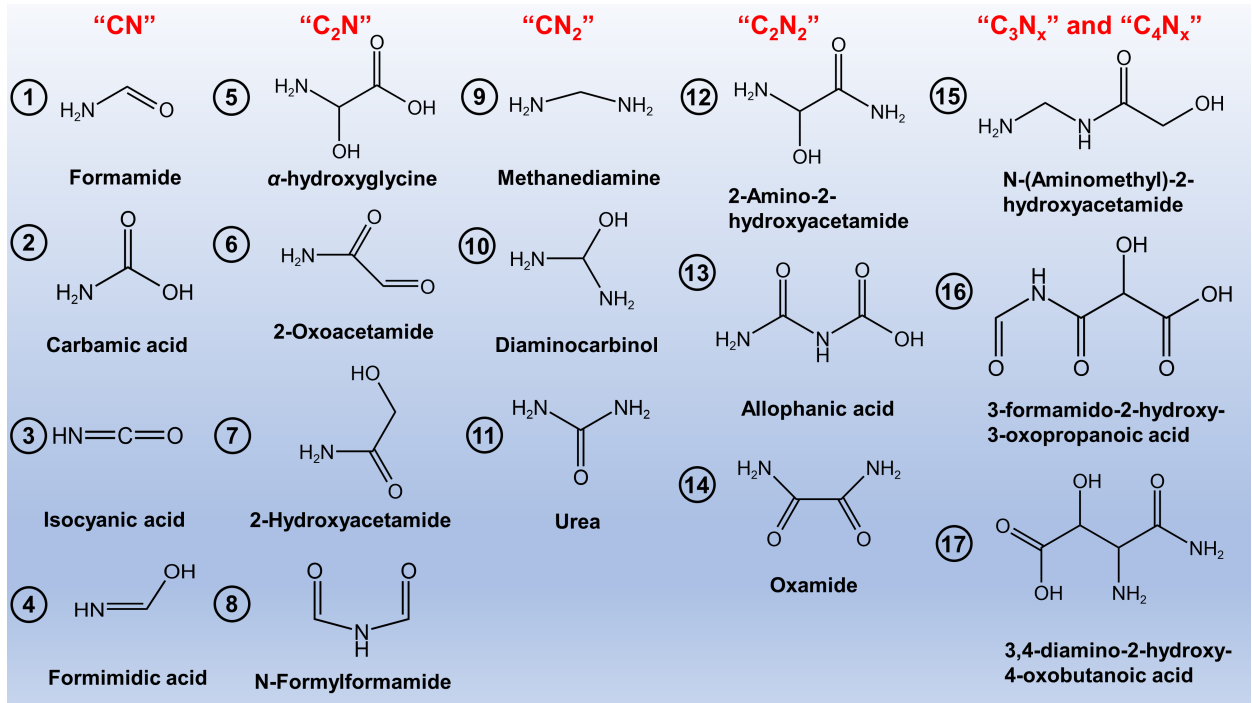
- [51] Ferus, M. *et al.* High-energy chemistry of formamide: A unified mechanism of nucleobase formation. *Proc. Natl. Acad. Sci.* **112**, 657–662 (2015).
- [52] Wang, L.-P. *et al.* Discovering chemistry with an ab initio nanoreactor. *Nat. Chem.* **6**, 1044–1048 (2014).
- [53] Gilbert, W. Origin of life: The RNA world. *Nature* **319**, 618–618 (1986).
- [54] Nisbet, E. Origin of life: RNA and hot-water springs. *Nature* **322**, 206–206 (1986).
- [55] McClain, W. H., Guerrier-Takada, C. & Altman, S. Model substrates for an RNA enzyme. *Science* **238**, 527–530 (1987).
- [56] Forster, A. C. & Altman, S. External guide sequences for an RNA enzyme. *Science* **249**, 783–786 (1990).
- [57] Breslow, R. On the mechanism of the formose reaction. *Tetrahedron Lett.* **1**, 22–26 (1959).
- [58] Drew, K. N., Zajicek, J., Bondo, G., Bose, B. & Serianni, A. S. ¹³C-Labeled aldopentoses: detection and quantitation of cyclic and acyclic forms by heteronuclear 1D and 2D NMR spectroscopy. *Carbohydr. Res.* **307**, 199–209 (1998).
- [59] Dewick, P. M. *Essentials of organic chemistry: for students of pharmacy, medicinal chemistry and biological chemistry* (John Wiley & Sons, 2013).
- [60] Dass, A. V. *et al.* Equilibrium and non-equilibrium furanose selection in the ribose isomerisation network. *Nat. Commun.* **12**, 2749 (2021).
- [61] Kolb, V. M. & Zhu, W. Complexes of ribose with silicates, borates, and calcium: Implications to astrobiology. In *Instruments, Methods, and Missions for Astrobiology VIII*, vol. 5555, 70–77 (SPIE, 2004).
- [62] Lambert, J. B., Lu, G., Singer, S. R. & Kolb, V. M. Silicate complexes of sugars in aqueous solution. *J. Am. Chem. Soc.* **126**, 9611–9625 (2004).
- [63] Ferus, M. *et al.* High-energy chemistry of formamide: A simpler way for nucleobase formation. *J. Phys. Chem. A* **118**, 719–736 (2014).

- [64] Choe, J. C. Mechanism of Prebiotic Uracil Synthesis from Urea and HC3O^+ in Space. *Astrobiology* **22**, 1363–1369 (2022).
- [65] Mojzsis, S. J. *et al.* Evidence for life on Earth before 3,800 million years ago. *Nature* **384**, 55–59 (1996).
- [66] Brenner, A. R. *et al.* Paleomagnetic evidence for modern-like plate motion velocities at 3.2 Ga. *Sci. Adv.* **6**, eaaz8670 (2020).
- [67] Korenaga, J. Initiation and evolution of plate tectonics on Earth: theories and observations. *Annu. Rev. Earth Planet. Sci.* **41**, 117–151 (2013).
- [68] Holder, R. M. & Viete, D. R. The metamorphic rock record through earth’s history. In *Reference Module in Earth Systems and Environmental Sciences* (Elsevier, 2024).
- [69] Blichert-Toft, J. & Albarède, F. Hafnium isotopes in Jack Hills zircons and the formation of the Hadean crust. *Earth Planet. Sci. Lett.* **265**, 686–702 (2008).
- [70] Hopkins, M., Harrison, T. M. & Manning, C. E. Low heat flow inferred from > 4 Gyr zircons suggests Hadean plate boundary interactions. *Nature* **456**, 493–496 (2008).
- [71] Huang, G., Mitchell, R. N., Palin, R. M., Spencer, C. J. & Guo, J. Barium content of Archaean continental crust reveals the onset of subduction was not global. *Nat. Commun.* **13**, 6553 (2022).
- [72] Aulbach, S. & Stagno, V. Evidence for a reducing Archean ambient mantle and its effects on the carbon cycle. *Geology* **44**, 751–754 (2016).
- [73] Holm, N. G. & Neubeck, A. Reduction of nitrogen compounds in oceanic basement and its implications for HCN formation and abiotic organic synthesis. *Geochem. Trans.* **10**, 1–11 (2009).
- [74] Néri, A., Guyot, F., Reynard, B. & Sotin, C. A carbonaceous chondrite and cometary origin for icy moons of Jupiter and Saturn. *Earth Planet. Sci. Lett.* **530**, 115920 (2020).
- [75] Nettelmann, N. *et al.* Uranus evolution models with simple thermal boundary layers. *Icarus* **275**, 107–116 (2016).

- [76] Postberg, F. *et al.* Macromolecular organic compounds from the depths of Enceladus. *Nature* **558**, 564–568 (2018).
- [77] Waite Jr, J. H. *et al.* Liquid water on Enceladus from observations of ammonia and ^{40}Ar in the plume. *Nature* **460**, 487–490 (2009).
- [78] Tosi, F. *et al.* Salts and organics on Ganymede’s surface observed by the JIRAM spectrometer onboard Juno. *Nat. Astron.* **8**, 82–93 (2024).
- [79] Gygi, F. Architecture of Qbox: A scalable first-principles molecular dynamics code. *IBM J. Res. Dev.* **52**, 137–144 (2008).
- [80] Perdew, J. P., Burke, K. & Ernzerhof, M. Generalized gradient approximation made simple. *Phys. Rev. Lett.* **77**, 3865–3868 (1996).
- [81] Spanu, L., Donadio, D., Hohl, D., Schwegler, E. & Galli, G. Stability of hydrocarbons at deep Earth pressures and temperatures. *Proc. Natl. Acad. Sci.* **108**, 6843–6846 (2011).
- [82] Cheng, B., Hamel, S. & Bethkenhagen, M. Thermodynamics of diamond formation from hydrocarbon mixtures in planets. *Nat. Commun.* **14**, 1104 (2023).
- [83] Zhang, Z., Sun, Y. & Wentzcovitch, R. M. PBE-GGA predicts the $\text{B8} \leftrightarrow \text{B2}$ phase boundary of FeO at Earth’s core conditions. *Proc. Natl. Acad. Sci.* **120**, e2304726120 (2023).
- [84] Hamann, D. Optimized norm-conserving vanderbilt pseudopotentials. *Phys. Rev. B* **88**, 085117 (2013).
- [85] Bussi, G., Donadio, D. & Parrinello, M. Canonical sampling through velocity rescaling. *J. Chem. Phys.* **126**, 014101 (2007).
- [86] Darve, E., Rodríguez-Gómez, D. & Pohorille, A. Adaptive biasing force method for scalar and vector free energy calculations. *J. Chem. Phys.* **128**, 144120 (2008).
- [87] Sidky, H. *et al.* SSAGES: software suite for advanced general ensemble simulations. *J. Chem. Phys.* **148**, 044104 (2018).

TABLE I. Classification of the CN-containing species and the selected molecules.

CN-containing	Selected molecules
“CN”	CH_2NO , CH_2NO_2 , CH_3NO , CH_3NO_2 , $\text{CH}_4\text{NO}\dots$
“ C_2N ”	$\text{C}_2\text{H}_2\text{NO}_2$, $\text{C}_2\text{H}_3\text{NO}$, $\text{C}_2\text{H}_3\text{NO}_2$, $\text{C}_2\text{H}_4\text{NO}$, $\text{C}_2\text{H}_4\text{NO}_3$, $\text{C}_2\text{H}_5\text{NO}_2$, $\text{C}_2\text{H}_5\text{NO}_3\dots$
“ CN_2 ”	CH_4N_2 , CH_6N_2 , CH_7N_2 , $\text{CH}_4\text{N}_2\text{O}\dots$
“ C_2N_2 ”	$\text{C}_2\text{H}_2\text{N}_2\text{O}_3$, $\text{C}_2\text{H}_3\text{N}_2\text{O}_2$, $\text{C}_2\text{H}_3\text{N}_2\text{O}_3$, $\text{C}_2\text{H}_4\text{N}_2\text{O}_2$, $\text{C}_2\text{H}_4\text{N}_2\text{O}_3$, $\text{C}_2\text{H}_5\text{N}_2$, $\text{C}_2\text{H}_5\text{N}_2\text{O}$, $\text{C}_2\text{H}_5\text{N}_2\text{O}_2$, $\text{C}_2\text{H}_6\text{N}_2\text{O}_2$, $\text{C}_2\text{H}_7\text{N}_2\text{O}_2\dots$
“ C_3N_x ” (“ $x = 1, 2, 3\dots$ ”)	$\text{C}_3\text{H}_2\text{NO}_5$, $\text{C}_3\text{H}_3\text{NO}_3$, $\text{C}_3\text{H}_4\text{NO}_3$, $\text{C}_3\text{H}_4\text{NO}_4$, $\text{C}_3\text{H}_4\text{NO}_5$, $\text{C}_3\text{H}_6\text{N}_2\text{O}_2$, $\text{C}_3\text{H}_7\text{N}_2\text{O}_2$, $\text{C}_3\text{H}_8\text{N}_2\text{O}_2\dots$
“ C_4N_x ”	$\text{C}_4\text{H}_3\text{NO}_5$, $\text{C}_4\text{H}_4\text{NO}_4$, $\text{C}_4\text{H}_4\text{NO}_5$, $\text{C}_4\text{H}_4\text{N}_2\text{O}_4$, $\text{C}_4\text{H}_6\text{N}_2\text{O}_3$, $\text{C}_4\text{H}_7\text{N}_2\text{O}_4\dots$


 FIG. 1. Chemical structures of the representative products for the “CN”, “ C_2N ”, “ CN_2 ”, “ C_2N_2 ”, “ C_3N_x ” and “ C_4N_x ” species.

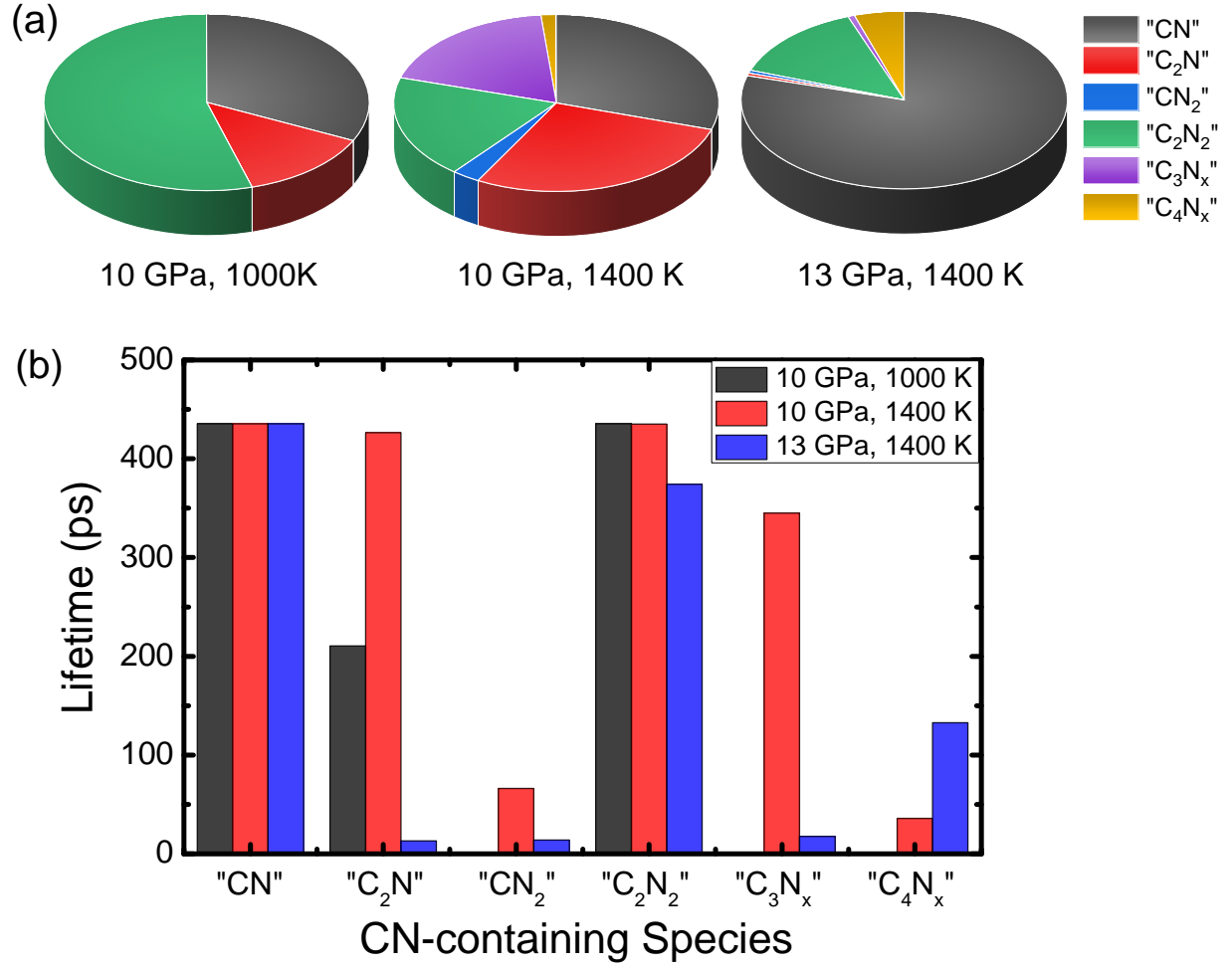


FIG. 2. CN-containing species at three P-T conditions. (a) Fractions and (b) average lifetime of the six CN-containing species obtained from AIMD simulations.

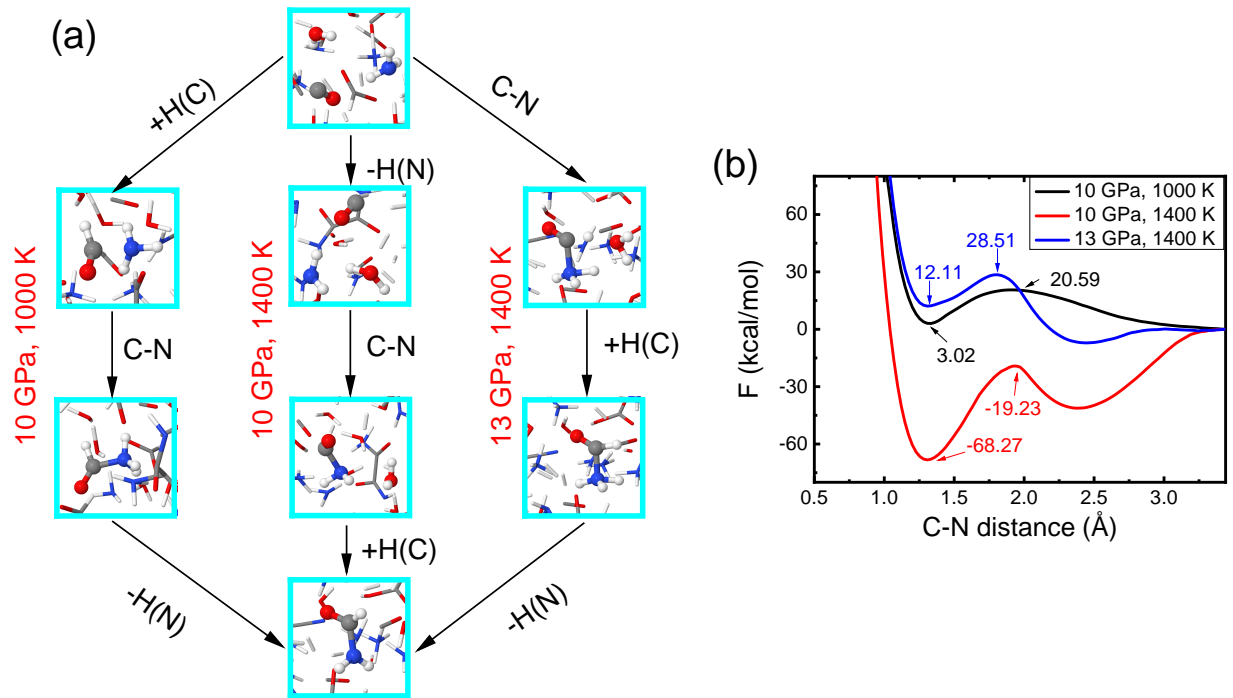


FIG. 3. Synthesis of formamide from H_2O , H_2 , CO , and NH_3 at three P-T conditions. There were initially 15 molecules for each of these four small molecules in the simulation box. **(a)** The key reaction steps. The labels over arrows, +H(C), C-N, and -H(N), refer to the formation of a C-H bond, a C-N bond, and the breaking of a N-H bond, respectively. **(b)** The free energies obtained at three P-T conditions as functions of the C-N distance.

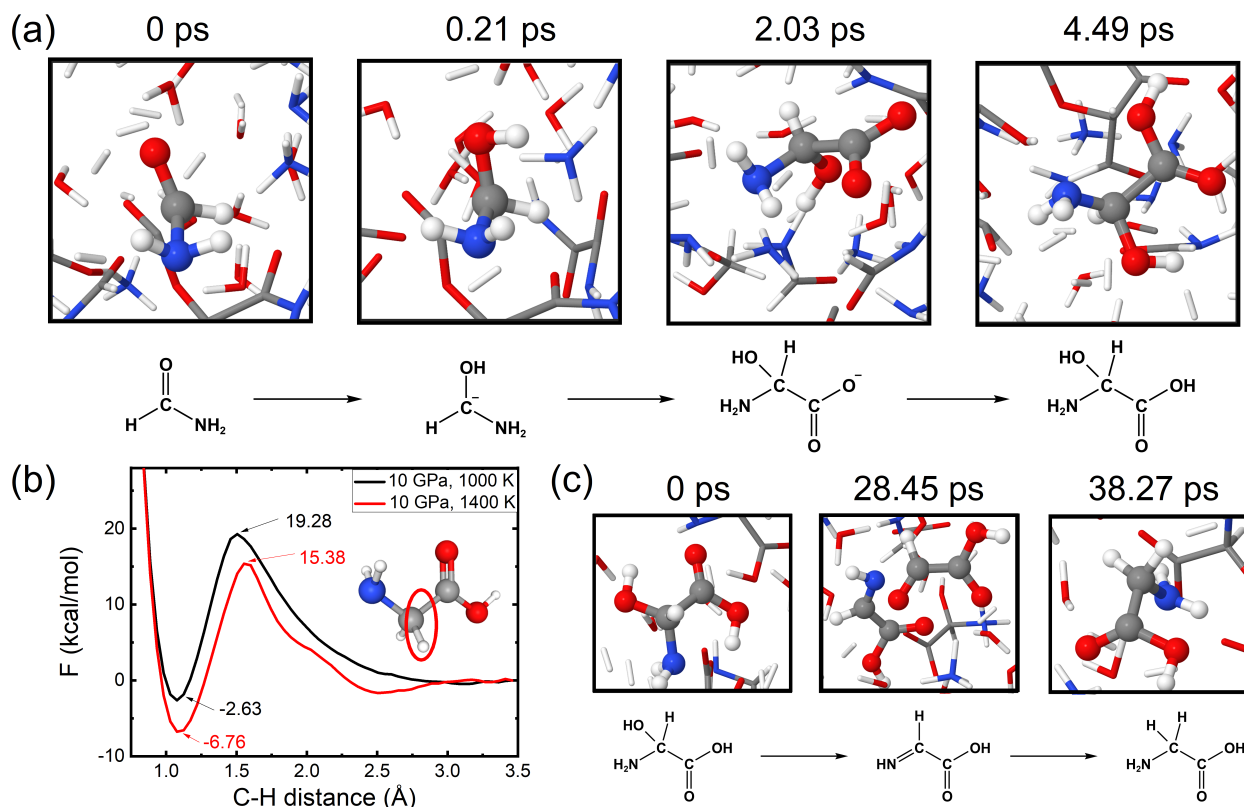


FIG. 4. Synthesis of α -hydroxyglycine and glycine at 10 GPa and 1400 K. (a) Key reaction steps in the formation of α -hydroxyglycine from formamide. (b) Free energies at two P-T conditions as functions of the C-H distance. (c) Key reaction steps in the formation of glycine from 5 α -hydroxyglycine, 10 H_2 , and 10 H_2O .

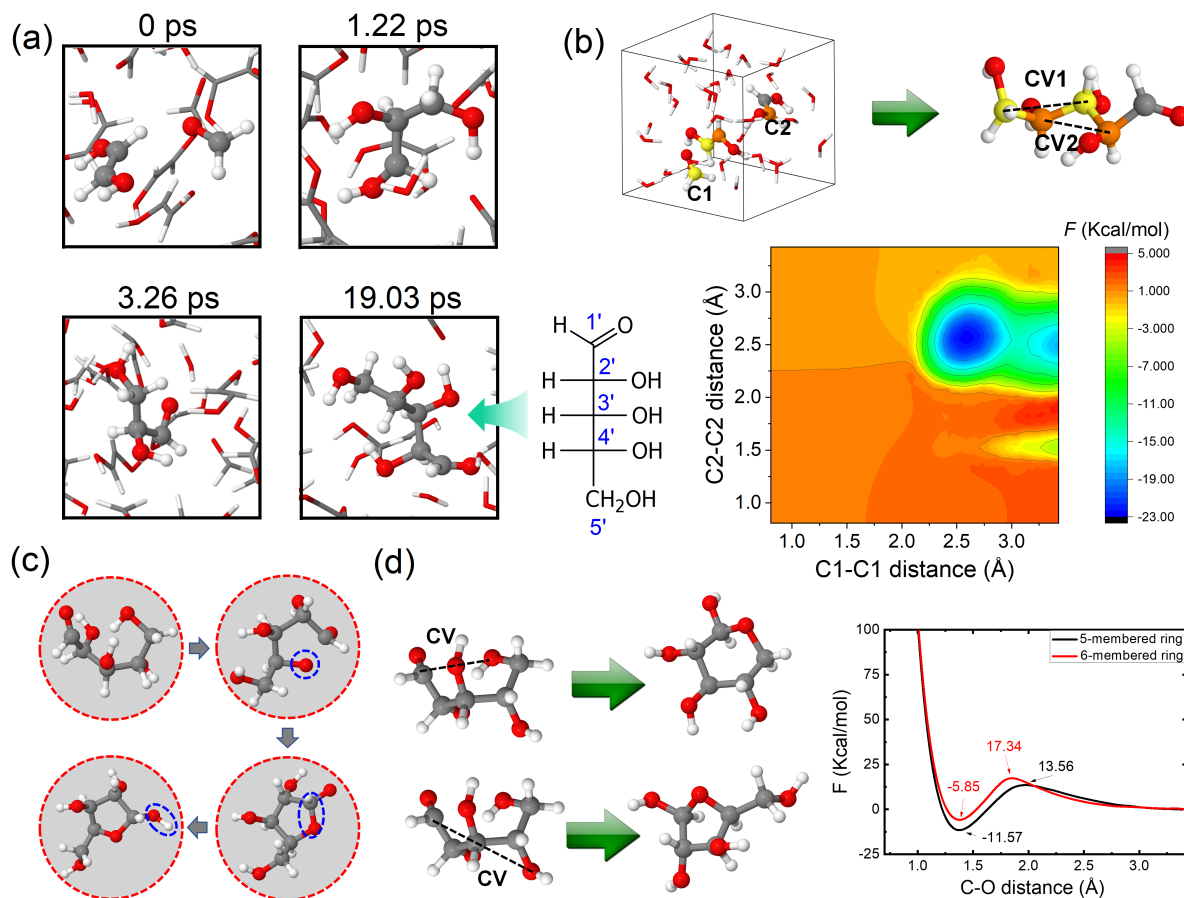


FIG. 5. Synthesis of ribose at 10 GPa and 1400 K. **(a)** Key reaction steps in the formation of the open-chain ribose from 10 (Z)-ethene-1,2-diol, 5 formaldehyde, and 5 H_2O . **(b)** The free energy landscape for the formation of ribose. Two C-C distances are the collective variables. To distinguish the selected carbon atoms, C1 and C2 are marked by yellow and orange colors, respectively. **(c)** The transformation of ribose from open chain to five-membered ring. **(d)** Free energies of the formation of furanose (five-membered ring) and pyranose (six-membered ring) forms of ribose. The C-O distance is the collective variable.

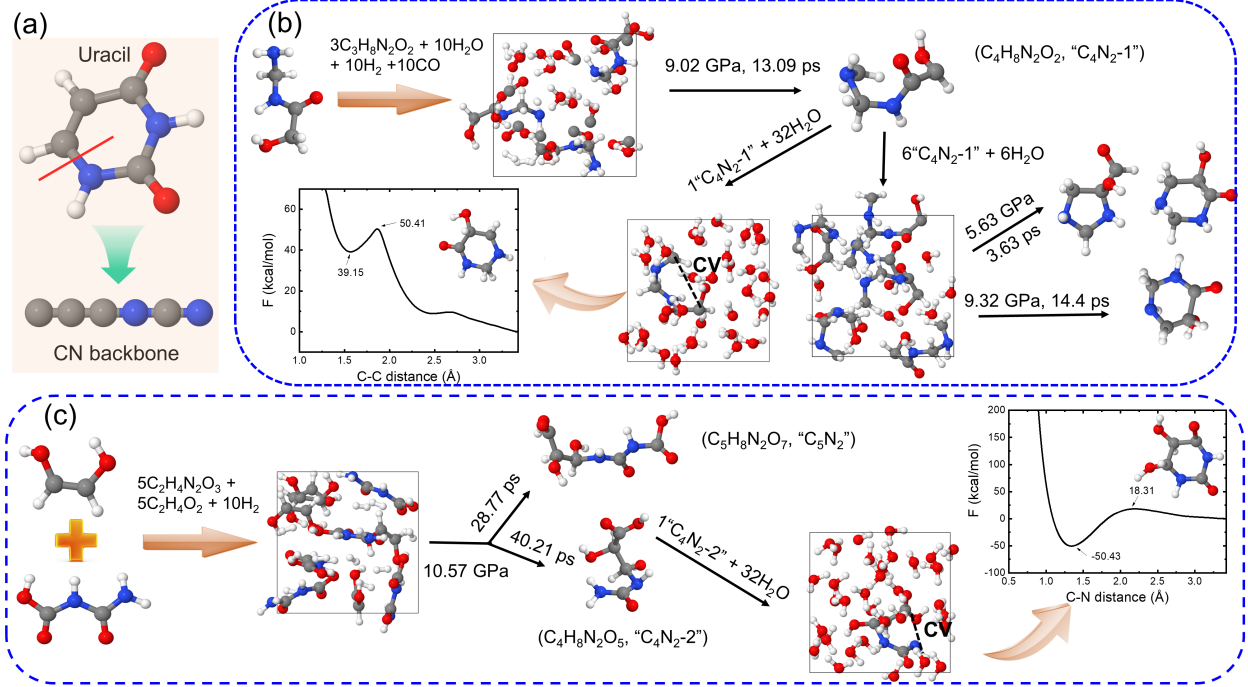


FIG. 6. Synthesis of uracil-like molecules at 10 GPa and 1400 K. (a) Structure of the uracil molecule and its CN-backbone when the C-N bond is broken. (b) The formation of the "C₄N₂-1" molecule with the same CN-backbone as the open-chain form of uracil. The reactants are 3 C₃H₈N₂O₂, 10 H₂O, 10 H₂, and 10 CO molecules in the simulation box. We further put 6 "C₄N₂-1" and 6 H₂O molecules in the simulation box to study the ring formation in the uracil molecule. The free energy calculation was conducted in the simulation box containing one "C₄N₂-1", and 32 H₂O molecules. (c) The formation of the "C₄N₂-2" molecule with the same CN-backbone as the open-chain form of uracil. The reactants are 5 C₂H₄N₂O₃, 5 C₂H₄O₂, and 10 H₂ molecules. The free energy calculation was conducted in the simulation box containing one "C₄N₂-2" and 32 H₂O molecules.